Enhanced chemistry-climate feedbacks in past greenhouse worlds

David J. Beerling[a,1], Andrew Fox[a,2], David S. Stevenson[b], and Paul J. Valdes[c]

[a]Department of Animal and Plant Sciences, University of Sheffield, Sheffield S10 2TN, United Kingdom; [b]School of GeoSciences, University of Edinburgh, Edinburgh EH9 3JN, United Kingdom; and [c]Department of Geographical Sciences, University of Bristol, Bristol BS8 1SS, United Kingdom

Edited by Ralph J. Cicerone, National Academy of Sciences, Washington, DC, and approved April 26, 2011 (received for review February 11, 2011)

Trace greenhouse gases are a fundamentally important component of Earth's global climate system sensitive to global change. However, their concentration in the pre-Pleistocene atmosphere during past warm greenhouse climates is highly uncertain because we lack suitable geochemical or biological proxies. This long-standing issue hinders assessment of their contribution to past global warmth and the equilibrium climate sensitivity of the Earth system (E_{ss}) to CO_2. Here we report results from a series of three-dimensional Earth system modeling simulations indicating that the greenhouse worlds of the early Eocene (55 Ma) and late Cretaceous (90 Ma) maintained high concentrations of methane, tropospheric ozone, and nitrous oxide. Modeled methane concentrations were four- to fivefold higher than the preindustrial value typically adopted in modeling investigations of these intervals, even after accounting for the possible high CO_2-suppression of biogenic isoprene emissions on hydroxyl radical abundance. Higher concentrations of trace greenhouse gases exerted marked planetary heating (>2 K), amplified in the high latitudes (>6 K) by lower surface albedo feedbacks, and increased E_{ss} in the Eocene by 1 K. Our analyses indicate the requirement for including non-CO_2 greenhouse gases in model-based E_{ss} estimates for comparison with empirical paleoclimate assessments, and point to chemistry-climate feedbacks as possible amplifiers of climate sensitivity in the Anthropocene.

biogenic aerosols | coals | stratosphere-troposphere exchange

Atmospheric CO_2 is the most important greenhouse gas (GHG) being affected by anthropogenic activities today (1). In addition to CO_2, methane (CH_4), tropospheric ozone (O_3), and nitrous oxide (N_2O) are all important noncondensing trace atmospheric GHGs (2), that contribute to the total terrestrial greenhouse effect by being highly efficient (on a per molecule basis) at absorbing infrared radiation from Earth's surface relative to CO_2 (1, 2). Methane contributes to additional planetary warming through its involvement in tropospheric photochemistry leading to ozone formation, and its oxidation in the lower stratosphere generates water vapor that acts as a highly effective GHG (2). Polar ice core records of Earth's past atmospheric composition indicate that the concentrations of both CH_4 and N_2O underwent significant variations on glacial-interglacial timescales (3), and on millennial timescales since the last glacial maximum (4). By extension, these paleoclimate records suggest significantly higher concentrations of trace GHGs existed during pre-Pleistocene episodes of extreme greenhouse warmth (5), particularly during the late Paleocene and early Eocene when sedimentary records indicate methane-producing wetland environments were extensive (6, 7). However, quantitative evaluation of the role that trace GHGs have played in climate change throughout Earth's history remains a major scientific challenge owing to the lack of geological or biological proxies.

Here, we report a three-dimensional (3D) Earth systems modeling approach that resolves trace GHGs concentrations through process-based representation of the terrestrial, climatic, and atmospheric processes involved in regulating Earth's atmospheric chemistry (8). Our 3D Earth systems model comprises the Hadley Centre climate model (HadCM3L) (9), widely used for future climate change prediction, coupled to the updated tropospheric chemistry-transport model STOCHEM (10) and the Sheffield Dynamic Global Vegetation Model (SDGVM) for simulating terrestrial vegetation biogeography, structure, and productivity (11). We focus on resolving the concentration of GHGs in the atmosphere, and quantifying their influence on the planetary energy budget, during two significant greenhouse climate intervals in Earth history over the past 100 million years (Ma)—the early Eocene (55 Ma) and the late Cretaceous (90 Ma). Our analyses for the early Eocene include assessment of the influence trace GHGs exert on the Earth system sensitivity (E_{ss}), a quantity central to future climate change prediction that incorporates slow (e.g., ice sheet disintegration and vegetation migration) and fast (e.g., clouds, aerosols, and trace gases) feedback processes (12, 13).

Simulations of both eras employed specified atmospheric CO_2 concentration of 4× the preindustrial (PI) CO_2 concentration of 280 ppm (1,120 ppm), as indicated by proxy evidence (14, 15), but with PI concentrations of all other trace GHGs. We undertook a further suite of chemistry-climate calculations for the early Eocene with $2 \times CO_2$ atmospheric concentration (560 ppm), as suggested by the lower bound of some proxies (14), to allow assessment of the effect of trace GHGs in modifying E_{ss}. Our analyses effectively identify the concentration, and climate feedback, of trace GHGs compatible when a particular atmospheric CO_2 concentration is specified as an external boundary condition.

Results and Discussion

Chemical Composition of the Ancient Atmosphere. Simulated baseline (i.e., control) land surface Eocene and Cretaceous greenhouse climates (Fig. S1), terrestrial vegetation properties, and hydrology (Fig. S2) significantly enhanced production and emission of biogenic trace gas emissions to the atmosphere relative to the PI situation (Fig. 1 and Table S1). Modeled methane emissions by wetland ecosystems far exceeded those for the PI (Fig. 1*A*), reflecting their wider geographical distribution especially in the Northern Hemisphere compared to the PI and the warm, moist, climates that stimulated emission rates (Fig. 1*B*). The simulated extensive Eocene wetlands are in general agreement with independent sedimentary evidence indicating widespread distribution of lignites and coal throughout North America and Eurasia in the late Paleocene and Eocene (16–18). A CO_2 doubling in the early Eocene (2× to 4× PI CO_2) enhanced wetland methane emissions by 44%, directly through CO_2 fertilization of terrestrial primary production, and indirectly through

Author contributions: D.J.B. and P.J.V. conceived and designed research; D.J.B., A.F., and P.J.V. performed research; D.J.B., A.F., D.S.S., and P.J.V. analyzed data; and D.J.B. wrote the paper.

The authors declare no conflict of interest.

This article is a PNAS Direct Submission.

Freely available online through the PNAS open access option.

[1]To whom correspondence should be addressed. E-mail: d.j.beerling@sheffield.ac.uk.

[2]Present address: National Ecological Observatory Network (NEON), National Center for Atmospheric Research (NCAR), 1685 38th Street, Suite 100, Boulder, CO 80301.

This article contains supporting information online at www.pnas.org/lookup/suppl/doi:10.1073/pnas.1102409108/-/DCSupplemental.

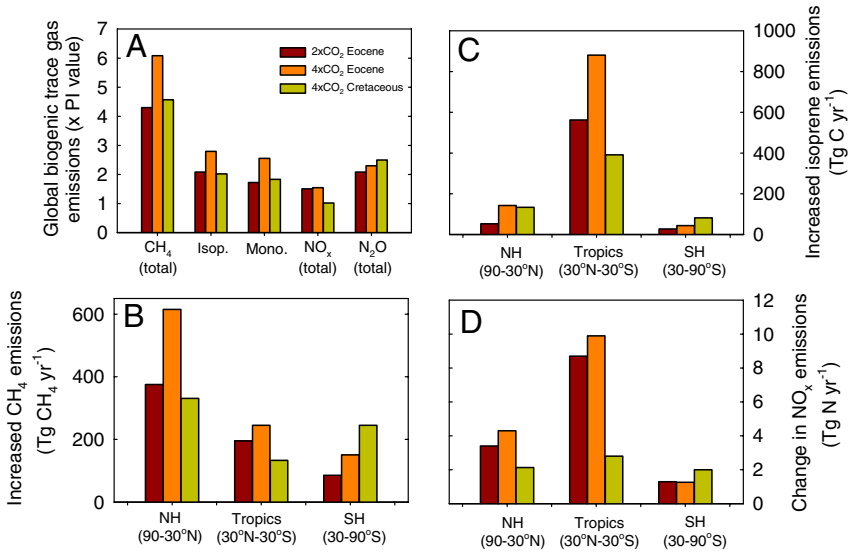

Fig. 1. Terrestrial ecosystem emissions of reactive trace gases in the Eocene and Cretaceous. Simulated equilibrium global-scale (*A*) reactive biogenic trace gas emissions to the atmosphere for the $2 \times CO_2$ (560 ppm) and $4 \times CO_2$ (1,120 ppm) Eocene, and $4 \times CO_2$ Cretaceous climates, relative to the preindustrial (PI) era. Panels *B*, *C*, and *D*, respectively, show zonal total fluxes for methane (CH_4) from all biogenic sources (wetlands, biomass burning, oceans, and termites), isoprene released from forested regions, and oxides of nitrogen ($NO_x = NO + NO_2$) released from soils, and generated by biomass burning and lightning (see *SI Text, SI Methods*).

positive climate feedbacks on wetland methane cycling (Fig. 1). This response points to a possible mechanism supplying additional radiative forcing during past episodes of strong and rapid warming and rising CO_2 levels (19).

Emissions of the long-lived GHG nitrous oxide also increased (Fig. 1) through enhanced terrestrial nitrogen cycling in past greenhouse climates, especially in the warm subtropics and tropics. The terrestrial carbon and nitrogen cycles of vegetation and soils are coupled in SDGVM through the Century model of soil nutrient cycling (11, 20). Litter, wood, and fine roots, add carbon and nitrogen to the soil, with the active pools of carbon being microbial, and the slow and passive pools having turnover rates of decades to millennia. Loss of litter from vegetation to the soil depletes the carbon stock of vegetation, but adds nitrogen to the soil that can be made available for plant uptake following microbial breakdown (11). Our calculations of soil biogenic N_2O fluxes utilize empirical functions describing the effects of soil moisture, temperature, soil nitrogen status, and net primary production (NPP) (21), that respond to warmer, wetter climates, and higher NPP and soil N status arising from climate and CO_2 fertilization effects.

Calculated equilibrium concentrations of trace GHGs (CH_4, O_3, and N_2O) for the Eocene and Cretaceous provide information on the chemical state of the atmosphere at times in Earth history tens of millions of years older than ice core records (Table 1). They indicate substantially higher concentrations of GHGs than those of the PI era that have typically been adopted in the past two decades of modeling Cretaceous and Eocene greenhouse climates (e.g., 22–24) (Table 1). Substantial modeled wetland CH_4 emissions sustained equilibrium atmosphere CH_4 concentrations (2,580–3,614 ppb) (Table 1) considerably higher than the PI value (700–750 ppb), with an upper value double the current concentration (approximately 1,800 ppb) (1). Methane lifetime, defined as the total atmospheric CH_4 burden divided by the sum of all loss processes (25), also increased (Table 1). It reflects a four- to fivefold higher CH_4 burden that was only partially offset by faster oxidation with hydroxyl radicals (OH) in a warmer climate, and increased OH production in the warm moist tropospheres (26) (Table 1) (Tables S2–S4). These CH_4 budget changes produced global mean concentrations of around 3,614 ppb in the $4 \times CO_2$ Eocene, and 3,304 ppb in the $4 \times CO_2$ Cretaceous (Table 1).

Table 1. Simulated trace greenhouse gases in early Eocene (55 Ma) and late Cretaceous (90 Ma) atmospheres

	[CH_4] (ppb)	CH_4 lifetime (yrs)	$\Delta H_2O_{[strat]}$ (%/ppm)	[surface O_3] (ppb)	[OH] (ppt)	[N_2O] (ppb)
Simulation						
Preindustrial (PI, 0 Ma)						
$1 \times CO_2$ (280 ppm)	695 (635–700)	7.1	not applicable	11.8	0.05	278 (275–280)
Early Eocene (55 Ma)						
$2 \times CO_2$ (560 ppm)	2,580	7.9	+25%/1.5 ppm	17.7	0.039	373
$2 \times CO_2$ (PI isoprene flux)	2,384	7.2		15.7	0.043	373
$4 \times CO_2$(1,120 ppm)	3,614	7.8	+40%/3.0 ppm	19.3	0.035	323
$4 \times CO_2$ (PI isoprene flux)	3,305	7.1		16.8	0.040	323
Late Cretaceous (90 Ma)						
$4 \times CO_2$ (1,120 ppm)	3,304	9.1	+40%/3.0 ppm	20.1	0.036	426

Values are for the troposphere unless otherwise indicated. Values are annual means for the last 12 months of each simulation after reaching equilibrium. Increases in stratospheric water vapor at an altitude of 40–50 km were estimated from two-dimensional chemical transport model calculations (27) with a surface methane concentration of 3,400 ppb, and are given as both a % and absolute increase, relative to the PI. N_2O is unreactive in the troposphere, with a long atmospheric lifetime of approximately 150 years (2). Tropospheric N_2O concentrations are calculated from the sum of the sources (from soils and biomass burning) and sinks and a 1D atmospheric model (see *SI Text, SI Methods*). Values in parentheses under the PI results indicate independent estimates (2).

Surface ozone concentrations were 63% and 70% higher in the $4 \times CO_2$ early Eocene and late Cretaceous simulations, respectively, relative to the PI (Table 1). In the case of the Eocene, increases of 15–20 ppb over large regions of the northern hemisphere were evident linked to the presence of isoprene-emitting forests (Fig. 2 *A* and *B* and Table 1). In the preanthropogenic atmosphere, tropospheric ozone is regulated by the photochemical oxidation of biogenic volatile organic compounds, particularly isoprene and also methane, in the presence of sufficient oxides of nitrogen ($NO_x = NO$ and NO_2) (28). Eocene and Cretaceous forests under the warm climates produced potentially high isoprene emissions, and greater tropical convection enhanced NO_x production by lightning (approximately 10 $Tg\,N\,yr^{-1}$ vs. 6.8 $Tg\,N\,yr^{-1}$ for the PI) (Fig. 1). Fluxes of isoprene and NO_x combined to increase net tropospheric ozone production and offset enhanced photochemical destruction related to the warm humid atmosphere (Table 1). Enhanced stratosphere-to-troposphere exchange (STE) flux due to a strengthening in the Brewer–Dobson circulation provided an additional source of ozone, with the global STE flux rising from 470 $Tg\,O_3\,yr^{-1}$ in the PI to 640 $Tg\,O_3\,yr^{-1}$ and 740 $Tg\,O_3\,yr^{-1}$ in the $4 \times CO_2$ Eocene and Cretaceous simulations (Table S4), respectively, a change similar to that calculated for end of the 21st century (29).

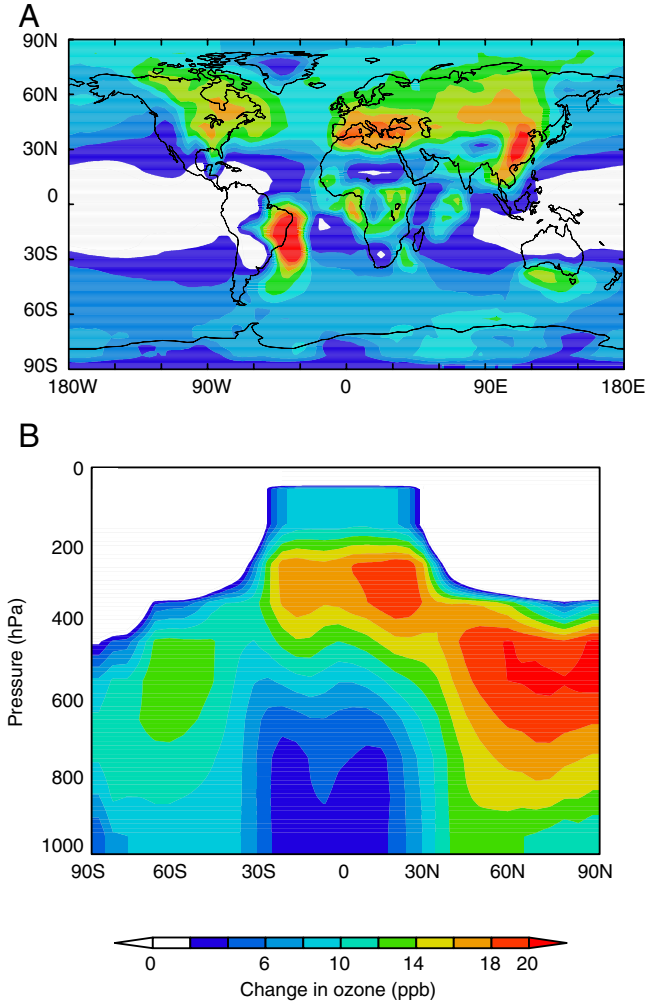

Fig. 2. Elevated surface ozone concentrations in the Eocene compared to the preindustrial world. Simulated increases in (*A*) mean annual surface level ozone for the $4 \times CO_2$ Eocene simulation and (*B*) the cross-sectional zonal average profile through the atmosphere. Ozone increases in (*A*) and (*B*) are relative to the preindustrial control simulation. Note in (*A*) changes in ozone fields are plotted over the present-day continental geography.

Uncertainties in the surface ozone calculations include the nonlinear inhibitory effect of elevated atmospheric CO_2 on isoprene emissions from terrestrial vegetation (30, 31) and the ongoing debate concerning atmospheric chemistry of isoprene interactions with OH (32, 33). We quantified the potential impacts of the former effect for 2× and $4 \times CO_2$ Eocene simulations by repeating the 3D Earth system chemistry-climate calculations with terrestrial biospheric isoprene fluxes reduced by approximately 60% (i.e., equivalent to that for the preindustrial), but with the fluxes of all other reactive trace gases maintained as before. This modification produced widespread declines in surface ozone of 3–5 ppb over continental and oceanic regions, and a global reduction of approximately 2 ppb (Table 1), as obtained in idealized analyses of high CO_2 inhibition of isoprene emissions on projections of future surface ozone concentrations (34). Isoprene affects the oxidizing capacity of the troposphere by consuming/regenerating OH radicals and hence influences methane chemistry (28, 32, 33). In our two simulations that included CO_2 inhibition of biogenic isoprene emissions, average methane concentrations decreased by approximately 300 ppb and methane lifetimes by 8–9% respectively. Uncertainty in CO_2 inhibition of isoprene emissions is, therefore, not an overriding influence on our atmospheric methane results (Table 1). Inclusion of enhanced HO_x radical recycling during isoprene oxidation, especially important in low NO_x environments (33), could reduce methane lifetimes and concentrations.

Climate Feedbacks by Elevated Trace Greenhouse Gas Concentrations. Elevated trace GHG concentrations contributed an estimated positive forcing of approximately 1.7–2.3 $W\,m^{-2}$ (Table S5) in addition to that of CO_2 and produced equilibrium climate system responses resulting in widespread significant warming, especially in the high latitudes (Figs. 3 and 4). This positive climate feedback is greater than expected from the additional forcing alone, due to amplification by reduced surface albedo through melting of continental snow and decreased sea-ice coverage, especially in the wintertime. Polar amplification of warming arises because the initial baseline simulations underrepresent the warmth of ancient greenhouse climates. Because this issue continues to affect all coupled ocean-atmosphere models (e.g., 22–24), the warming (Fig. 3) represents the expression of positive biotic feedback mechanisms missing from earlier simulations of these climates obtained with prescribed PI concentrations of trace GHGs.

Overall, ecosystem-driven changes in chemistry induced climate feedbacks that increased global mean annual land surface temperatures by 1.4 and 2.7 K for the 2× and $4 \times CO_2$ Eocene simulations, respectively, and 2.2 K for the Cretaceous (Fig. 3 *E* and *F*). The relative contribution of each trace GHG to increased Eocene and Cretaceous land temperatures at $4 \times CO_2$, assessed with multiple separate coupled-ocean atmosphere HadCM3L model simulations, revealed methane and associated increases in stratospheric water vapor dominate, with nitrous oxide and tropospheric ozone contributing approximately equally to the remainder (Fig. 3 *E* and *F*). Although amplification of warming by our simulated high concentrations of trace gas concentrations is significant and widespread, especially during the wintertime at high latitudes on both the land and the oceans (Fig. 4), it is insufficient to substantially close the gap between the modeled climate and proxy temperature data in the high latitudes. For these comparisons, we assembled proxy data for the Paleocene–Eocene Thermal Maximum (55 Ma) and early Eocene Climatic Optimum (53–50 Ma), and for peak late Cretaceous warmth (94–89 Ma) (Fig. 4 and *SI Text*). However, the time constraints for the Eocene were relaxed to include the important and extensive dataset for the early middle Eocene from fossil plants (35), even though these data probably underrepresent peak early Eocene warmth.

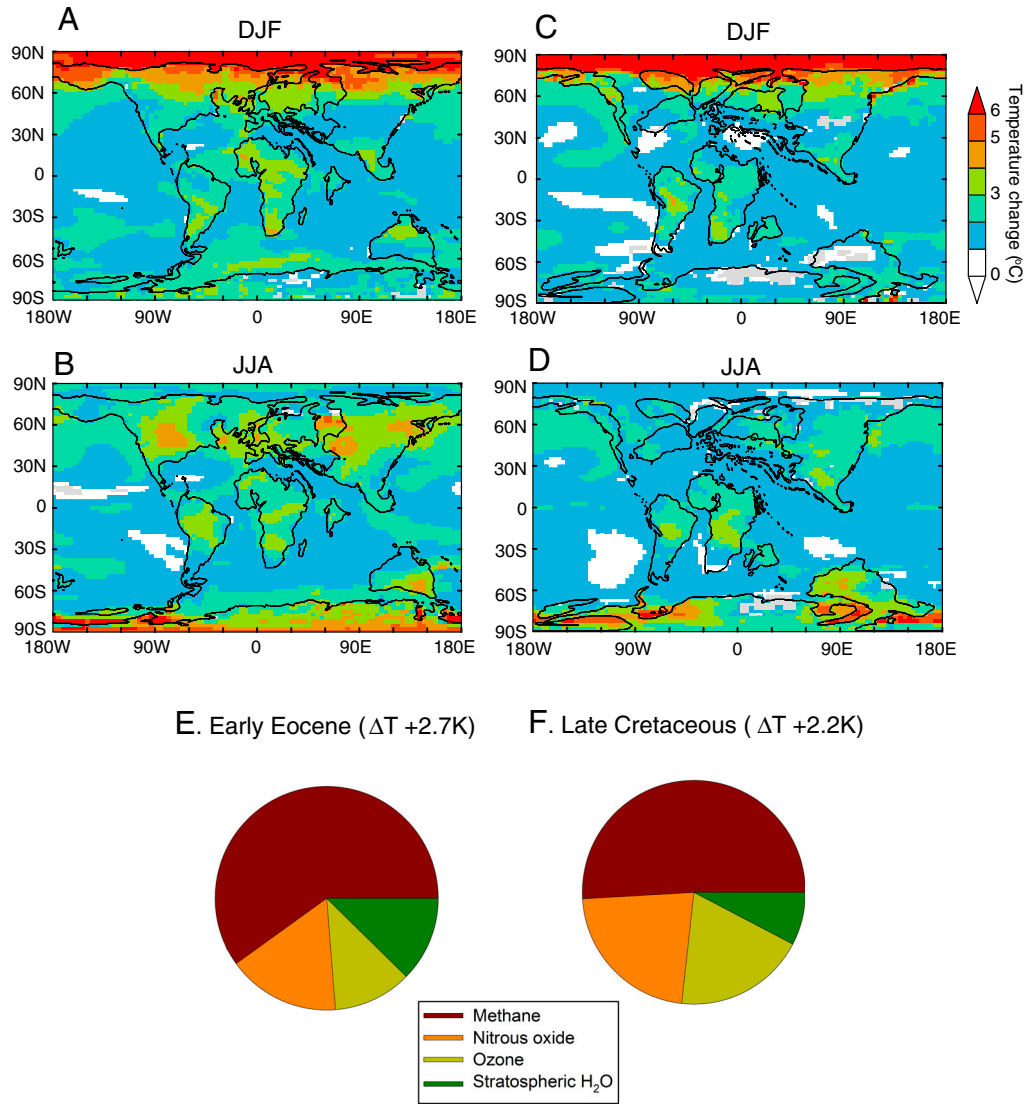

Fig. 3. Enhanced chemistry-climate feedbacks in past greenhouse worlds. Simulated equilibrium surface temperature increases (ΔT) by elevated trace greenhouse gas concentrations (Table 1) on the $4\times CO_2$ Eocene (*A*, *B*) and $4\times CO_2$ Cretaceous (*C*, *D*) during northern hemisphere winter (DJF) and northern hemisphere summer [June July August (JJA)] climates respectively. Feedbacks were quantified with the coupled ocean-atmosphere GCM HadCM3L by prescribing PI and elevated levels of trace GHGs (Table 1). Only temperature differences exceeding 95% confidence limits are displayed. (*E*) and (*F*) indicate the relative contribution of each greenhouse gas to land surface mean annual temperature increases in the Eocene and Cretaceous respectively.

Amplification of warming is slightly more marked in the Eocene relative to the Cretaceous simulations (Fig. 4 *B* and *F*) due to the Eocene control simulation being cooler in wintertime (Fig. S1). This allows more extensive seasonal sea ice and snow cover in the Eocene, which in turn promotes greater positive surface-melting albedo feedbacks (Fig. 4). The cooler state of the Eocene control climate, even with similar CO_2 concentrations is related to differing paleogeography, especially that the Cretaceous represents a relatively high stand in sea-level and hence the global land surface fraction is smaller. In addition, the early Eocene paleogeographies have a relatively enclosed Arctic that promotes colder high latitude conditions. The extent to which there was seasonal sea-ice and snow cover in the Eocene can be debated. There is evidence for ice-rafted debris in the middle Eocene (36), but there is no suggestion of sea-ice in the early Eocene.

In the Eocene, mean annual land surface temperatures indicated by the proxies are generally reproduced by the model, whereas those in the oceans remain cooler than suggested by the proxy evidence by 10–25 °C (Fig. 4 *A* and *C*). A similar situation exists for the late Cretaceous (Fig. 4 *E* and *G*). The apparent ability of HadCM3 to better reproduce terrestrial rather than marine proxy temperature data may reflect a cool bias in temperature estimates from fossil leaves that can arise from assemblages derived from wet microenvironments (e.g., swamps and riparian zones) (37), and a possible warm bias in the marine proxies. In addition, there are potentially different processes controlling marine and terrestrial temperatures in the model. Away from the coasts, modeled terrestrial climate is sensitive to the atmospheric circulation, and particularly processes that affect the albedo, such as land surface conditions, and clouds. The latter are notoriously difficult to model but their representation may be sufficient in these time periods. However, the model is failing to reproduce the equator-to-pole temperature gradient in the ocean, which will be linked to the ocean heat transport. This may be related to the relatively poor resolution of the ocean component of most coupled climate models. Nevertheless, the persistent, long-standing, mismatch between model and data climates raises the possibility that the models are missing fundamental physical or biological high latitude amplifying feedback processes.

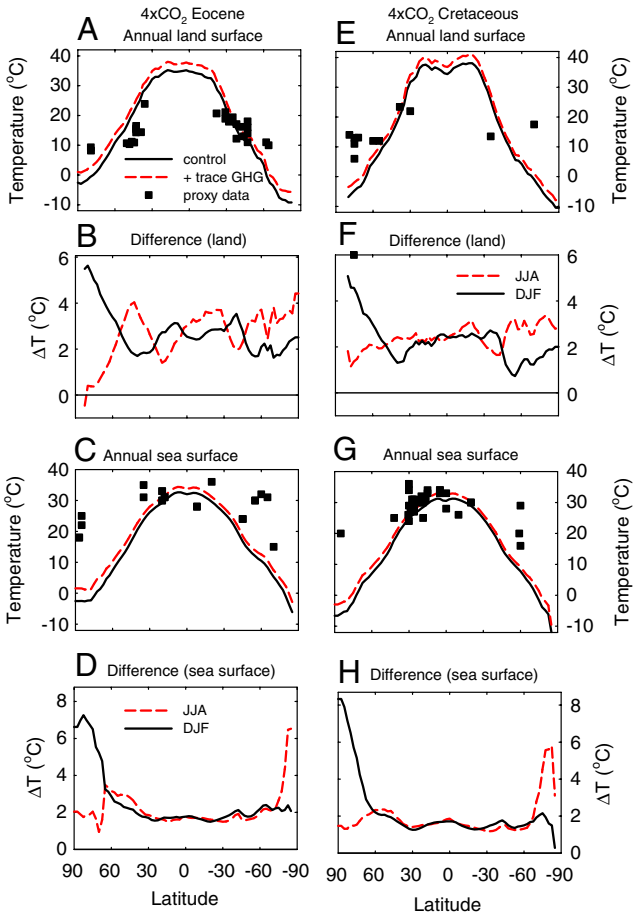

Fig. 4. Simulated latitudinal temperature gradients in the Eocene and Cretaceous. (*A*) Latitudinally averaged mean annual land surface temperature in the Eocene ($4 \times CO_2$ concentration) for the control runs (preindustrial concentrations of trace greenhouse gases, black line) and after inclusion of the positive feedback of elevated trace greenhouse gases (red line). (*B*) Changes in latitudinally averaged seasonal mean annual land surface temperature due to forcing by elevated trace greenhouse gas concentrations relative to the control simulation. JJA; June, July, August; DJF; December, January, February. (*C*) and (*D*) as (*A*) and (*B*) but for sea-surface temperature. (*E–H*) Equivalent plots as for *A–D*, but for the $4 \times CO_2$ Cretaceous simulations. Proxy data sources for panels *A*, *C*, *E* and *G* are given in *SI Text*.

In the Eocene, higher reactive trace gas emissions, driven by a doubling in the atmospheric CO_2 concentration from 2× to 4× PI values, produced a climatic feedback that increased the E_{ss} by ca. 1 K to 4 K overall (Table 2), a value similar to that obtained in mid-Pliocene simulations (3.3–3.0 Ma) (13). Our results, therefore, strengthen the emerging view from empirical paleoclimate studies (13, 19, 38) that the Earth system has a high equilibrium climate sensitivity to a CO_2. Inclusion of the climatic effects arising from feedbacks due to ecosystem trace gas–chemistry interactions in modeling studies of past warm intervals in Earth history offers one mechanism for further rapprochement with empirical paleoclimate estimates of E_{ss}. However, accurately gauging this essential quantity with models requires assessment of the sign and strength of forest-related biogenic aerosol-cloud feedbacks, a developing area of Earth system modeling (39). Isoprene fluxes from the terrestrial biosphere during the Eocene and Cretaceous, with CO_2 suppression, are comparable to those of the preindustrial world (Table S1) and therefore their photochemical oxidation is unlikely to generate a significantly higher secondary organic aerosol (SOA) loading in the atmosphere over that of the PI to induce climatic cooling. However, the larger fluxes of other terpenes, particularly monoterpene, whose emissions from

Table 2. Simulated Eocene climate system response to atmospheric CO_2 and elevated concentrations of trace greenhouse gases (GHGs), and calculated Earth system sensitivity (E_{ss})

Simulation

	Global surface	Land surface	E_{ss}	E_{ss}
Early Eocene (55 Ma)	Temperature (K)	Temperature (K)	Global (K)	Land (K)
$2 \times CO_2$ (560 ppm)	293.3	291.8	—	—
$2 \times CO_2$ + GHGs	294.6	293.2	—	—
$4 \times CO_2$ (1,120 ppm)	296.5	296.0	3.2	4.2
$4 \times CO_2$ + GHGs	298.6	298.7	4.0	5.5

leaves are not known to be sensitive to elevated CO_2, could increase SOA formation (39). Understanding these feedbacks should be the focus of future research effort.

Limitations of the Chemistry Modeling. We recognize that a limitation of the Earth systems modeling approach reported here relates to our treatment of stratospheric chemistry. STOCHEM captures a reasonable representation of tropospheric chemistry (10), but does not include the full range of stratospheric ozone reactions. The model simulates stratosphere-to-troposphere transport of ozone by including a simple relaxation toward seasonally varying stratospheric ozone climatology above 100 hPa. The effects of colder stratospheric temperatures (caused by $2 \times CO_2$ and $4 \times CO_2$ concentrations), and elevated tropospheric concentrations of CH_4 and N_2O (Table 1), on stratospheric ozone concentrations are not included in our simulations. However, changes in circulation, in particular cross-tropopause mass (and ozone) fluxes (29), are represented (Table S4), as are changes in stratospheric H_2O associated with different levels of CH_4 (Table 1). Increased levels of N_2O can be expected to lead to stratospheric ozone depletion, and changes in the distribution/magnitude of stratospheric ozone will change tropospheric photolysis rates. Prather and Hsu (40) show that N_2O, CH_4, and O_3, are coupled in complex ways in simulations of the present-day atmosphere; this coupling will shift in different climates, and simulations with stratospheric chemistry-climate models are required to elucidate the full details. However, recent studies with a version of STOCHEM coupled to a full stratospheric chemistry scheme (41) indicate that the effects on tropospheric ozone are typically dominated by changes in stratosphere-troposphere exchange rather than changes in photolysis rates.

Nevertheless, we recognize that changes in CH_4 and N_2O reported here are likely to exert impacts in the stratosphere (40) that have yet to be accounted for. Along with the roles of isoprene emissions and chemistry, and biogenic aerosols, these all add uncertainties, and should be the subject of future modeling investigations into past greenhouse worlds.

Conclusions

Our Earth system simulations provide unique constraints on the possible range of trace GHG concentrations in the ancient atmosphere during past greenhouse periods in Earth history, a long-standing and previously highly uncertain boundary condition. These results emerge from the integration of models capturing interactions between the terrestrial biosphere, climate system and chemistry and deposition processes. Quantitative assessment of the associated atmospheric chemistry-climate feedbacks reveals substantial and widespread planetary heating during these intervals missing from earlier model estimates of E_{ss} (Figs. 3 and 4). These simulations for past greenhouse worlds contextualize projections of future emission scenarios by the Intergovernmental Panel on Climate Change. Projected future anthropogenic

trace gas emissions suggest humanity is likely to recreate atmospheric conditions in the Anthropocene (1, 2) not seen on Earth for the past 20–50 Ma, and that could increase Earth's longer-term climate sensitivity to rising atmospheric CO_2 concentrations.

Methods

The 3D Earth systems model comprises the HadCM3L climate model (9), widely used for future climate change prediction, coupled to the updated tropospheric chemistry-transport model STOCHEM (10) and the SDGVM for simulating terrestrial vegetation biogeography, structure, and productivity (11). Modeling procedures are initiated by simulating global baseline climate and vegetation properties from which appropriate biogenic trace gas emission schemes provide monthly fluxes to STOCHEM for computing the equilibrium atmospheric chemistry from HadCM3L 3D meteorology. In intermodel comparisons, STOCHEM compares favorably with other chemistry schemes in terms of its predicted changes in tropospheric ozone concentrations (42), indicating its utility for the present study. All of the simulations used the fully coupled atmosphere-ocean version of HadCM3L.

An enhancement to the capability of the full Earth system modeling strategy reported here is the continued iterative feedback between trace GHGs and climate, vegetation processes, trace gas fluxes, and chemistry, until equilibrium between the component modules is reached. This enhancement, and incorporation of SDGVM land surface vegetation-climate feedbacks, makes the individual modules fully self-consistent under the prescribed CO_2 regime. Our Earth systems approach to modeling the chemical composition of past atmospheres is verified by earlier successful simulations of the observed preindustrial methane concentration (650 ppb), and polar ice-core records of methane during the last glacial maximum, 21 ka (412 ppb) (8), and over the last 130 ka (43), with markedly different boundary conditions, including ice sheets, sea-level, atmospheric CO_2 and vegetation.

ACKNOWLEDGMENTS. We thank Oliver Wild and Nick Hewitt for helpful comments on the manuscript, David Wilton for technical support, Dan Schrag for earlier discussions on this work, and the Leverhulme Trust for funding. This work was carried out using the computational facilities of the Advanced Computing Research Centre, University of Bristol (http//www.bris.ac.uk/acrc). D.J.B. and P.J.V. gratefully acknowledge funding through receipt of Royal Society–Wolfson Research Merit Awards.

1. Lacis AA, Schmidt GA, Rind D, Rudy RA (2010) Atmospheric CO_2: principal control knob governing Earth's temperature. *Science* 330:356–459.
2. Forster P, et al. (2007) *Climate Change 2007: The Physical Science Basis* (Cambridge University Press, Cambridge), pp 129–234.
3. Spahni R, et al. (2005) Atmospheric methane and nitrous oxide of the late Pleistocene from Antarctic ice cores. *Science* 310:1317–1321.
4. Flückiger J, et al. (2004) N_2O and CH_4 variations during the last glacial epoch: Insight into global processes. *Global Biogeochem Cy* 18:GB1020 10.1029/2003GB002122.
5. Zachos JC, Dickens GR, Zeebe RE (2008) An early Cenozoic perspective on greenhouse warming and carbon-cycle dynamics. *Nature* 451:279–283.
6. Sloan LC, et al. (1992) Possible-methane induced polar warming in the early Eocene. *Nature* 357:320–322.
7. Beerling DJ, et al. (2009) Methane and the CH_4-related greenhouse effect over the past 400 million years. *Am J Sci* 309:97–113.
8. Valdes PJ, Beerling DJ, Johnson CE (2005) The ice age methane budget. *Geophys Res Lett* 32:L02704 10.1029/2004GL021004.
9. Pope VD, et al. (2000) The impact of new physical parametrizations in the Hadley Centre climate model: HadAM3. *Clim Dynam* 16:123–146.
10. Stevenson D, et al. (2005) Impacts of climate change and variability on tropospheric ozone and its precursors. *Faraday Discuss* 130:41–57.
11. Beerling DJ, Woodward FI (2001) *Vegetation and the Terrestrial Carbon Cycle. Modelling the First 400 Million Years* (Cambridge University Press, Cambridge).
12. Hansen J, et al. (2008) Target CO_2: where should humanity aim? *Open Atmos Sci J* 2:217–231.
13. Lunt DJ, et al. (2010) Earth system sensitivity inferred from Pliocene modelling and data. *Nat Geosci* 3:60–64.
14. Breecker DO, Sharp ZD, McFadden LD (2010) Atmospheric CO_2 concentrations during ancient greenhouse climates were similar to those predicted for A.D. 2100. *Proc Natl Acad Sci USA* 107:576–580.
15. Fletcher BJ, et al. (2008) Atmospheric carbon dioxide linked to Mesozoic and early Cenozoic climate change. *Nat Geosci* 1:43–48.
16. Duff PMD (1987) Mesozoic and Tertiary coals: A major world energy resource. *Mod Geol* 11:29–50.
17. Warwick PD, Stanton RW (1988) Depositional models for 2 tertiary coal-bearing sequences in the Powder River Basin, Wyoming, USA. *J Geol Soc* 145:613–620.
18. Nagy J (2005) Delta-influenced foraminiferal facies and sequence stratigraphy of Paleocene deposits in Spitsbergen. *Palaeogeogr Palaeoclimatol Palaeoecol* 222:161–179.
19. Zeebe RE, Zachos JC, Dickens GR (2009) Carbon dioxide forcing alone insufficient to explain Palaeocene-Eocene thermal maximum warming. *Nat Geosci* 2:576–580.
20. Parton WJ, et al. (1993) Observations and modeling of biomass and soil organic carbon matter dynamics for the grassland biomass worldwide. *Global Biogeochem Cy* 7:785–809.
21. Bouwman A, et al. (1993) Global analysis of the potential for N_2O production in natural soils. *Global Biogeochem Cy* 7:557–597.
22. Barron EJ, Peterson WH (1989) Model simulation of the Cretaceous ocean circulation. *Science* 244:684–686.
23. Otto-Bliesner OL, Upchurch GR (1997) Vegetation-induced warming of high latitude regions during the Late Cretaceous Period. *Nature* 385:804–807.
24. Huber M, Caballero R (2003) Eocene El Nino: Evidence for robust tropical dynamics in the "hothouse". *Science* 299:877–881.
25. Lelieveld J, Crutzen PJ, Dentener F (1998) Changing concentration, lifetime, and climate forcing of atmospheric methane. *Tellus* B50:128–150.
26. Schmidt GA, Shindell DT (2003) Atmospheric composition, radiative forcing, and climate change as a consequence of a massive methane release from gas hydrates. *Paleoceanography* 18:PA000757 10.1029/2002PA000757.
27. Wuebbles DJ, Hayhoe KAS, Kotamarthi R (2000) *Atmospheric Methane* (Springer, Berlin), pp 304–341.
28. Fehsenfeld FC, et al. (1992) Emissions of volatile organic compounds from vegetation and their implications for atmospheric chemistry. *Global Biogeochem Cy* 6:389–430.
29. Hegglin MI, Shepherd TG (2009) Large climate-induced changes in ultraviolet index and stratosphere-to-troposphere ozone flux. *Nat Geosci* 2:687–691.
30. Possell M, Hewitt CN, Beerling DJ (2005) The effects of glacial atmospheric CO_2 concentrations and climate on isoprene emissions by vascular plants. *Global Change Biol* 11:60–63.
31. Monson RK, et al. (2007) Isoprene emissions from terrestrial ecosystems in response to global change: minding the gap between models and observations. *Philos T R Soc S-A* 365:1677–1695.
32. Lelieveld J, et al. (2008) Atmospheric oxidation capacity sustained by a tropical forest. *Nature* 452:737–740.
33. Archibald AT, et al. (2011) Impacts of HO_x regeneration and recycling in the oxidation of isoprene: Consequences for the composition of past, present and future atmospheres. *Geophys Res Lett* 38:L05804, 10.1029/2010GL046520.
34. Young PJ, Arneth A, Schurgers G, Zeng G, Pyle JA (2009) The CO_2 inhibition of terrestrial isoprene emission significantly affects future ozone projections. *Atmos Chem Phys* 9:2793–2803.
35. Greenwood DR, Wing SL (1995) Eocene continental climates and latitudinal temperature gradients. *Geology* 23:1044–1048.
36. Stickley CE, et al. (2009) Evidence for middle Eocene Arctic sea ice from diatoms and ice-rafted debris. *Nature* 460:376–379, 10.1038/nature08163.
37. Peppe DJ, et al. (2011) Sensitivity of leaf size and shape to climate: Global patterns and paleoclimatic applications. *New Phytol* 190:724–739.
38. Pagani M, Liu Z, LaRiviere J, Ravelo AC (2010) High Earth-system climate sensitivity determined from Pliocene carbon dioxide concentrations. *Nat Geosci* 3:27–30.
39. Kulmala M, et al. (2004) A new feedback mechanism linking forests, aerosols, and climate. *Atmos Chem Phys* 4:557–562.
40. Prather MJ, Hsu J (2010) Coupling of nitrous oxide and methane by global atmospheric chemistry. *Science* 330:952–954, 10.1126/science.1196285.
41. Tian W, et al. (2010) Effects of stratosphere-troposphere coupling on tropospheric ozone. *J Geophys Res* 115:D00M04, 10.1029/2009JD013515.
42. Stevenson DS, et al. (2006) Multi-model ensemble simulations of present-day and near-future tropospheric ozone. *J Geophys Res* 111:D08301, 10.1029/2005JD006338.
43. Singarayer JS, Valdes PJ, Friedlingstein P, Nelson S, Beerling DJ (2011) Late Holocene methane rise caused by orbitally controlled increase in tropical sources. *Nature* 470:82–85.